This is an open access article published under a Creative Commons Attribution (CC-BY) License, which permits unrestricted use, distribution and reproduction in any medium, provided the author and source are cited.

ACS AUTHORCHOICE

ACS OMEGA

http://pubs.acs.org/journal/acsodf

Article

Willow Catkins-Derived Porous Carbon Membrane with Hydrophilic Property for Efficient Solar Steam Generation

Shaochun Zhang, Linlin Zang, Tianwei Dou, Jinlong Zou, Yanhong Zhang,* and Liguo Sun*

Cite This: *ACS Omega* 2020, 5, 2878−2885

Read Online

ACCESS | Metrics & More | Article Recommendations | Supporting Information

ABSTRACT: Biomass wastes are abundant and common in our daily life, and they are cost-effective, promising, and renewable. Herein, collected willow catkins were used to prepare a hydrophilic biochar composite membrane, which was placed in a tree-like evaporation configuration to simulate a natural transpiration process. The strong light absorption (∼96%) of the biochar layer could harvest light and convert it into thermal energy, which then is used to heat the surrounding water pumped by a porous water channel via capillary action. A hydrophilic light-absorber layer remarkably increased the attachment sites of water molecules, thereby maximizing the use of thermal energy. At the same time, hierarchically porous structure and large specific surface area (∼1380 m^2 g^{-1}) supplied more available channels for rapid water vapor diffusion. The as-prepared composite membrane with a low-cost advantage realized a high evaporation rate (1.65 kg m^{-2} h^{-1}) only under 1 sun illumination (1 kW m^{-2}), which was improved by roughly 27% in comparison with the unmodified hydrophobic composite membrane. The tree-like evaporation configuration with excellent heat localization resulted in the evaporator achieving a high solar-to-vapor conversion efficiency of ∼90.5%. Besides, the composite membrane could remove 99.9% sodium ions from actual seawater and 99.5% heavy metal ions from simulated wastewater, and the long-term stable evaporation performance proved its potential in actual solar desalination. This work not only fabricated an efficient evaporator but also provided a strategy for reusing various natural wastes for water purification.

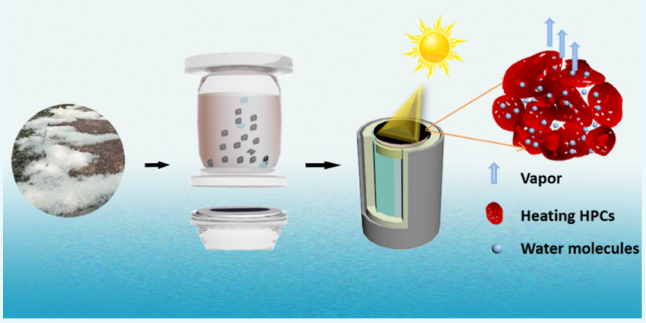

INTRODUCTION

Due to the lack of clean and safe water in the world, how to solve the crisis has become one of the most important focus in scientific research studies.[1−3] Desalination is an important technique for obtaining pure water from seawater. Generally, traditional desalination processes (such as membrane technologies, mechanical engines, and electrochemical devices) have large energy requirement and high cost. Sometimes, the processes could lead to environmental pollution.[4−6] As one of the most abundant renewable resource on the earth, solar energy can be collected and converted into thermal energy via various light absorbers. As a result, solar steam generation is expected to be an efficient method to produce pure water.[7−11] With respect to the conventional nanofluid system, energy cannot be completely utilized to heat the bulk water; therefore, the process usually involves considerable heat loss between the bulk water and outer environment.[12−15] As for another reported light absorbers, such as plasmonic nanoparticles,[16,17] graphene oxide, and carbon nanotubes,[18−21] they still face high cost and complicated preparation procedure, which significantly restrict their large-scale application in desalination.[22] Therefore, it is necessary to develop cost-effective materials with a high energy conversion efficiency.[23−25]

Natural biomass is widely founded in people's lives, and it has a huge potential application value as a renewable resource. Because of low cost, large specific surface area, and porous structure, biochar derived from the biomass have been utilized in energy storage, energy conversion, and environment remediation.[26−31] In recent years, the carbonized biomass has been considered as an effective light absorber in solar steam generation, and most of the studies have focused on only using the high-temperature carbonization method.[32−35] For example, wood-based evaporators with low tortuosity have a low evaporation rate due to a relatively thick light-absorbing layer via direct carbonization or flame treatment.[32] Therefore, they only achieved high evaporation rate and energy conversion efficiency under strong sun illumination, which could increase the cost and energy consumption in the practical application.[33,36−41] Liu's group directly carbonized lotus seedpods, which exhibited a lower evaporation rate of 1.3 kg m^{-2} h^{-1}.[42] Considering that the capillary action is inversely proportional to the pore size, the reasons of a low evaporation rate might be that the large pore size (>0.8 mm) of the petiole decreased the capillary action and water supply rate. Besides, when water was pumped into the

Received: November 2, 2019
Accepted: January 23, 2020
Published: February 5, 2020

© 2020 American Chemical Society

https://dx.doi.org/10.1021/acsomega.9b03718
ACS Omega 2020, 5, 2878−2885

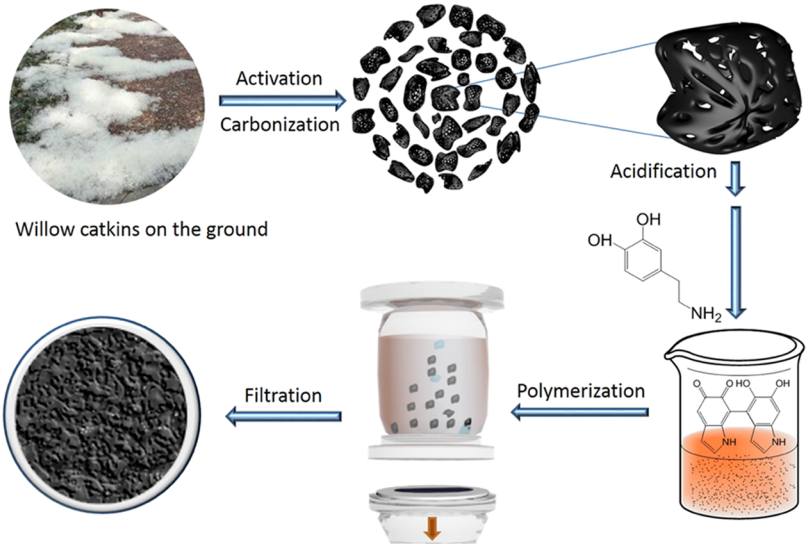

Figure 1. Schematic diagram of the preparation of the composite membrane.

receptacle, larger open pores (≈1 mm) on its surface might cause more heat dissipation according to Hu's report.[43] Zhu et al. used carbonized mushrooms with a well macroporous structure as a low-cost evaporator.[34] However, because of the existing problem similar to that of the wood-based evaporators, their evaporation rate and light-to-vapor conversion efficiency were only 1.5 kg m^{-2} h^{-1} and 78% under 1 sun illumination, respectively. To solve the above issues, Liu et al. utilized carbonized corn straw powders as a light-absorbing layer and then coated them on the surface of geopolymer-based support with excellent thermal insulation.[44] The result indicated that the mesoporous structure of the biomass can accelerate water transportation. Nevertheless, the low specific surface area (467 m^2 g^{-1}) just increased the evaporation rate to 1.58 kg m^{-2} h^{-1}. In view of this fact, only carbonization treatment and simply using a biomimetic channel structure cannot solve the problems of low evaporation rate and low energy conversion efficiency. Recently, some researchers have proposed that water from hydrophilic materials with porous structures had lower vaporization enthalpy than bulk water, which was beneficial for more effective energy utilization and a faster evaporation rate.[45−48] Therefore, limiting water to a thin evaporation layer and increasing the specific surface area and the hydrophilicity of light absorbers may be effective methods to improve evaporation performance.

Willow catkins are a kind of common natural waste in many large cities of China. In spring, a large number of catkins float in the air and lie on the roads, which may cause a fire hazard and worsen the air quality, even respiratory allergies. Owing to the hollow structure and large specific surface area of catkin fibers, they have been studied in energy storage and water treatment, such as supercapacitor electrodes and oil absorption materials.[49−52] So far, there are few reports about the use of carbonized catkins as photothermal materials for solar steam generation. Herein, our work prepared a hydrophilic polymer-modified biochar composite membrane via a simple three-step process. Through carbonizing willow catkins and pore former together, the biochar layer obtained a hierarchically porous structure, resulting in reducing light loss and accelerating vapor diffusion. Mixed acid treatment and polydopamine (PDA) modification can supply more hydrophilic functional groups on the biochar layer to increase contact sites with water molecules and then enhance evaporation performance. Moreover, a tree-like evaporation configuration, which has been proved to have excellent heat localization ability, was utilized to simulate the natural transpiration process and collect clean water.[53,54] As a result, the composite membrane exhibited a highly efficient solar steam generation and a stable desalination performance. This work proposed a novel strategy of reusing willow catkins, which could be very promising in solar desalination and water purification.

RESULTS AND DISCUSSION

A porous activated carbon prepared from willow catkins was modified by hydrophilic poly-dopamine,[55,56] which was formed into biochar composite membrane after filtration. A schematic diagram of the preparation of the composite membrane is shown in Figure 1.

Scanning electron microscopy (SEM) and transmission electron microscopy (TEM) images were taken to observe the porous structure and inner morphologies of the treated catkins. Figure 2a indicates that the porous carbon polyhedra (PCPs) had obvious and abundant pores after the activation and carbonization treatment, which was conducive for constructing

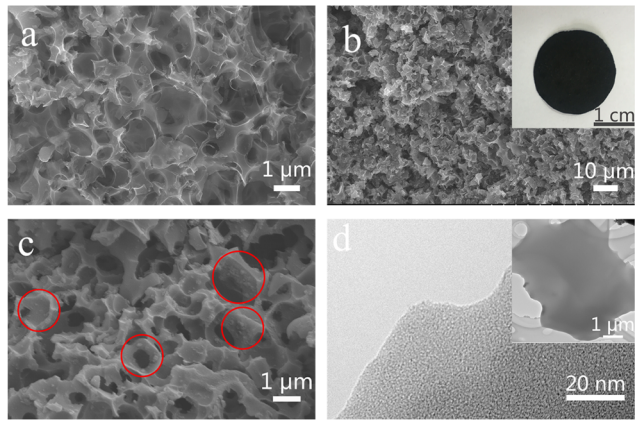

Figure 2. SEM image of (a) the PCPs and (b, c) the modified PCPs. The digital picture in the inset of (b) is the composite membrane with a diameter of 2 cm. (d) TEM image of modified PCPs.

https://dx.doi.org/10.1021/acsomega.9b03718
ACS Omega 2020, 5, 2878−2885

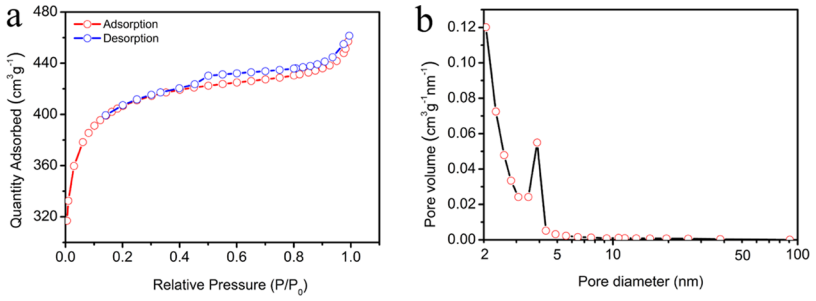

Figure 3. (a) Nitrogen adsorption−desorption isotherm. (b) Pore size distribution of modified PCPs.

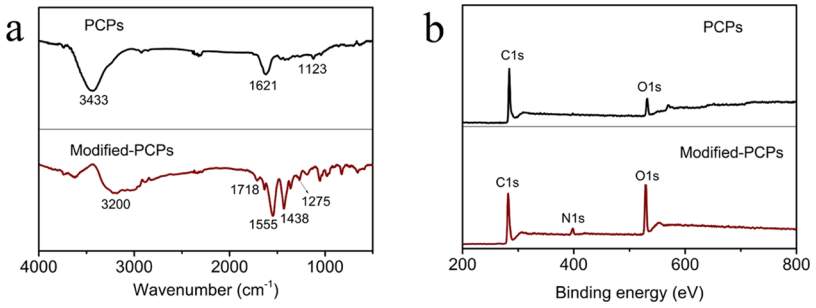

Figure 4. FTIR spectra (a) and XPS spectra (b) of PCPs and modified PCPs.

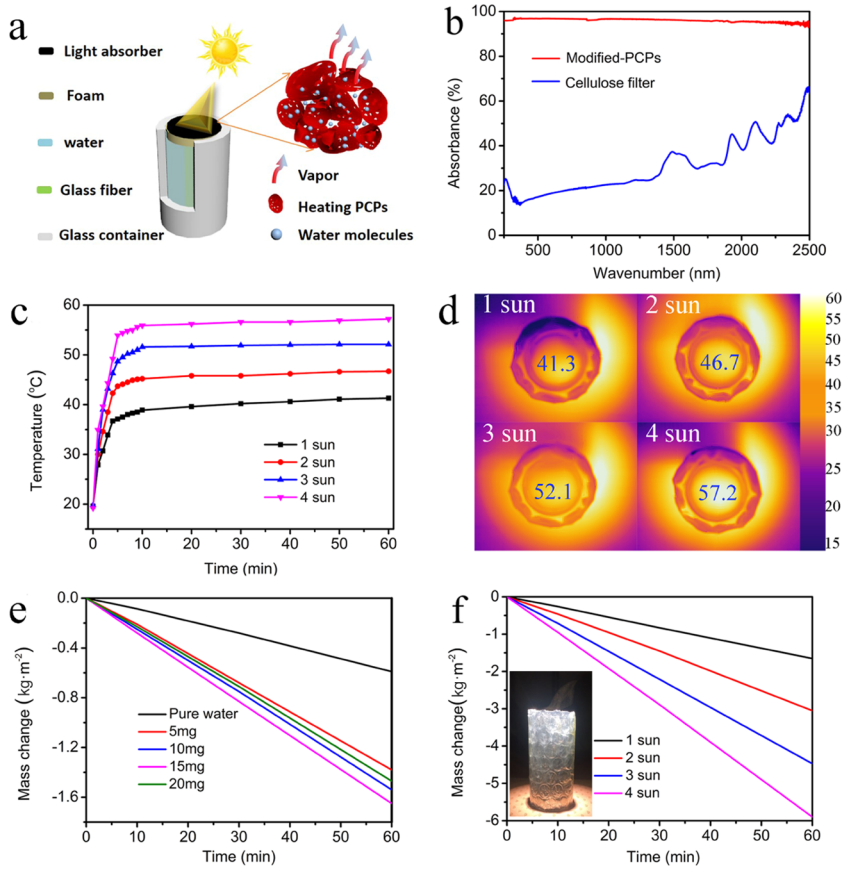

Figure 5. (a) Schematic illustration of solar steam generation with thermal insulation. (b) Absorbance spectra of cellulose filter and the composite membrane in the wavelength range of 250−2500 nm. (c) Surface temperature at different times of the composite membrane. (d) IR images after 60 min solar illumination under 1−4 sun illumination. (e) Water mass change for the composite membrane under 1 sun irradiation with 0−20 mg of modified PCPs. (f) Water mass change for the composite membrane with 15 mg of modified PCPs under 1−4 sun illumination. The inset is the digital photograph of the visible steam under 4 sun illumination.

https://dx.doi.org/10.1021/acsomega.9b03718
ACS Omega 2020, 5, 2878−2885

transpiration channels for water vapor. The digital picture in the inset of Figure 2b shows that the composite membrane had a black upper surface due to the biochar deposition, and the composite membrane still remained integrated after shaking several times (Movie S1). The SEM images (Figure 2b,c) present the surface and enlarged morphologies of modified PCPs, respectively, indicating the interconnected macroporous structure of the biochar layer. In comparison with the PCPs, many PDA particles were deposited on the surface of the modified PCPs and their porous structures were not destroyed after the PDA modification (red magnified parts in Figure 2c). The TEM image clearly shows that a thin slice of the biochar had a large number of mesoporous structures (Figure 2d).

To verify its porous structure and obtain the specific surface area, the modified PCPs were investigated by the nitrogen adsorption−desorption test (Figure 3). The isotherm curve was type IV with a hysteresis loop (Figure 3a), indicating the presence of microporous and mesoporous structures.[57] The result is consistent with the TEM image (Figure 2d). The Brunauer−Emmett−Teller (BET) surface area of the modified PCPs was calculated to be 1380 $m^2\ g^{-1}$, with the total pore volume of 0.7 $cm^3\ g^{-1}$. KOH has a strong activation capability for the willow catkins by reacting with carbon during the carbonization process, leading to the release of a gas product to introduce porosity, which resulted in a high specific surface area.[58−60] Figure 3b shows the distribution of mesopore diameters between 2 and 50 nm, and the average pore size of modified PCPs was about 2 nm. Figures 2 and 3 indicate that modified PCPs had a hierarchically porous structure, which was beneficial for enhancing light absorption and transportation of water molecules.[61]

Fourier transform infrared (FTIR) spectra were measured to investigate the functional groups of PCPs and modified PCPs (Figure 4a). The PCPs had two significant characteristic peaks at 3433 and 1621 cm^{-1}, corresponding to O−H groups and C═C of the aromatic ring, respectively.[28,50] After the polymerization process, the PCPs showed several new absorption peaks. Due to the effect of strong acid on the biochar, three peaks at 1718, 1555, and 1438 cm^{-1} were characteristic to the stretching vibration of C═O of −COO− groups.[62] Moreover, two peaks appearing at about 3200 and 1275 cm^{-1} corresponded to the N−H symmetric stretching vibration and the C−N stretching vibration from PDA, respectively.[55,63,64] In addition, X-ray photoelectron spectra (XPS) further confirmed the element compositions before and after PDA modification (Figure 4b). After the modification, the N 1s peak can be clearly observed in the XPS spectrum of modified PCPs, and the mass ratio of C/N decreased from 35.57 to 15.06 (Table S1), which proved that the PDA particles were successfully anchored on the carbonized catkins.

To further enhance the solar steam generation, we used a tree-like evaporation configuration to perform the entire experiment (Figure 5a). The composite membrane (thermal conductivity was 0.297 $W\ m^{-1}\ K^{-1}$) was placed on the upper surface of polystyrene foam (thermal conductivity was 0.035 $W\ m^{-1}\ K^{-1}$) floating on water to decrease the heat conduction to the bulk water. The hydrophilic glass-fiber paper across the foam could deliver the water to the composite membrane via capillary action. To determine the heat concentration performance, the light absorption of the black composite membrane was tested by a UV−vis−NIR spectrophotometer. Since the porous structure could reduce light loss by confining light in small caves,[65] the average absorption of the composite membrane can reach ∼96% in the wavelength range of 250−2500 nm, which was much higher than that of the pure cellulose membrane (Figure 5b). Due to the excellent light absorption performance, the surface of the membrane could rapidly increase from 19.6 to 41.3 °C within 10 min and then reach an equilibrium temperature under 1 sun illumination (Figure 5c). As the sun illumination intensity rose, the surface temperatures increased to 46.7, 52.1, and 57.2 °C under 2, 3, and 4 sun illumination after 60 min, respectively (Figure 5d).

Besides, hydrophilic water channels also contributed to improving solar evaporation performance. As shown in Figure S1, the modification treatment can remarkably decrease the water contact angle from 130 to 40°; meanwhile, it can also offer hydrophilic sites for a continuous grabbing of water molecules from surrounding channels. The hydrophilic channels had a larger gas−liquid contact surface and resulted in a more efficient solar water evaporation.[66−68] To confirm the result, unmodified PCPs and modified PCPs were loaded on the cellulose paper of the same area, and both of them had a loading mass of 15 mg each. The result indicated that the modified composite membrane had a larger mass loss after 60 min illumination under 1 sun (Figure S2), thereby proving that hydrophilic hierarchical pores were more conducive for a fast vapor diffusion. To determine the appropriate loading mass, different loading masses of modified PCPs were filtered on the cellulose paper of the same area. Figure 5e shows that the composite membrane had a higher water mass loss than the bulk water without any light absorber. However, the mass of light absorber was not directly proportional to the evaporation rate. When the loading mass increased from 5 to 15 mg, the evaporation rate went up from 1.38 to 1.65 $kg\ m^{-2}\ h^{-1}$. In contrast, the evaporation rate of the composite membrane with a loading mass of 20 mg dropped to 1.47 $kg\ m^{-2}\ h^{-1}$. This was because thicker light absorber layers could hinder the fast diffusion of water molecules. Therefore, we optimized the loading mass according to the data and used the composite membrane with a loading mass of 15 mg as an example in the following investigation. As we know, the optical concentration has a great effect on the surface temperature, which further affects the water evaporation rate. As shown in Figure 5f, the mass change witnessed a significant upward trend with the increasing light intensity. The water evaporation rates under 4 sun illumination could reach 5.90 $kg\ m^{-2}\ h^{-1}$, which was 3.5 times that under 1 sun illumination. The inset picture presents the visible steam on the surface of the composite membrane under 4 sun illumination (Movie S2). The above result indicated that the hydrophilic porous structure can not only rapidly absorb the water from the bulk and transport water molecule to the heating location but also supply large number of transpiration channels for a fast vapor diffusion.

The light-to-vapor energy conversion efficiency (ECE) was an important criterion to evaluate the evaporation performance of the materials. Therefore, we calculated the ECE value according to the following equation

$$\eta_{ECE} = \frac{\dot{m} h_{LV}}{C_{opt} P_0}$$

where $\dot{m}$ is the mass flux, h_{LV} is the total enthalpy of the liquid−vapor phase change, P_0 is the normal solar illumination of 1 sun (1 $kW\ m^{-2}$), and $C_{opt}P_0$ is the illumination intensity on the absorber surface.[22,53] In particular, the calculation of h_{LV} was based on the sensible heat- and temperature-dependent

https://dx.doi.org/10.1021/acsomega.9b03718
ACS Omega 2020, 5, 2878−2885

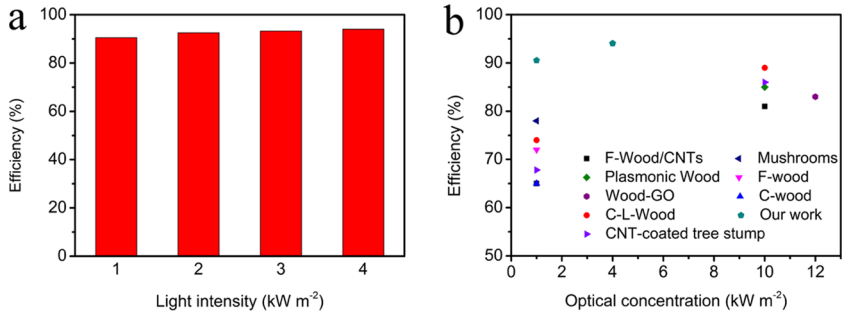

Figure 6. (a) Thermal conversion efficiency of a modified membrane with 15 mg of absorbers under 1−4 sun illumination. (b) Solar steam efficiencies of our work compared to other reports about the biomass materials.

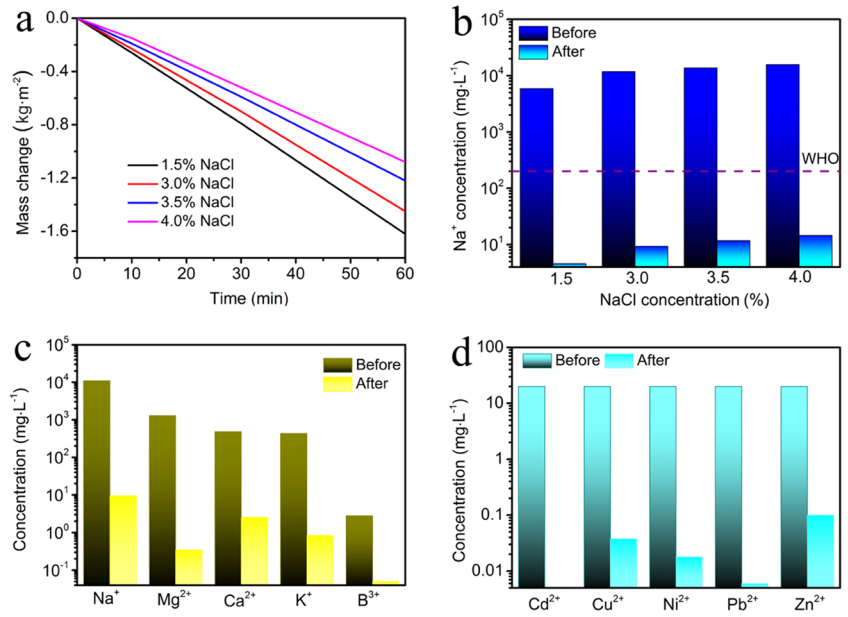

Figure 7. (a) Mass change of simulated seawater of different salinities. (b) Concentrations of Na^+ in the bulk water and filtrate. (c) Concentrations of five heavy-metal ions in the Bohai Sea and collected water. (d) Concentration changes of Cd^{2+}, Cu^{2+}, Ni^{2+}, Pb^{2+}, and Zn^{2+} in the simulated wastewater before and after purification. All tests were conducted under 1 sun illumination.

enthalpy of vaporization (Figure S3 and Table S2). The detailed calculation process is presented in the Supporting Information. The conversion efficiencies of the composite membrane gradually increased from 90.5 to 94.1% when the illumination increased from 1 to 4 sun (Figure 6a). We listed some of the reported light absorbers made by biomass materials (Figure 6b).[32,34−40] In most studies, researchers usually only used the intrinsic transport channels of natural materials without further treatment. Therefore, under 1 sun illumination, their evaporation rates were below 1.6 kg m^{-1} h^{-1}, and the corresponding efficiencies were lower than that of our work. Although some absorbers obtained excellent solar evaporation performance, they usually needed exposure to higher optical concentration.

Solar energy is a sustainable and pollution-free source that can be used to solve many serious global challenges, including desalination and wastewater treatment. Therefore, we studied the evaporation performance and salt rejection of the composite membrane in three kinds of bulk water, namely, simulated brine containing different concentrations of sodium chloride, actual seawater from the Bohai Sea (China) and wastewater containing heavy-metal ions. As shown in Figure 7a, the composite membrane can steadily produce clean water with an average rate of 1.62, 1.45, 1.22, and 1.08 kg m^{-2} h^{-1} when they treated simulated seawater with concentrations of 1.5, 3.0, 3.5, and 4.0% NaCl, respectively. During vaporization of actual seawater, the evaporation rate can reach up to 1.52 kg m^{-2} h^{-1} (Figure S4). Through collecting the condensed water in a glass container (Figure S5), the product water quality can be evaluated using inductively coupled plasma (ICP) technique. Figure 7b,c shows that most ions from the bulk solution were removed and the concentration of ions in the collected water was far lower than the standard of the World Health Organization (WHO). The evaporator can also remove 99.5% heavy-metal ions from simulated wastewater (Figures 7d and S6). The above results proved that the tree-like evaporator had excellent solar desalination and water treatment performances. Moreover, the long-term tests indicated that the composite membrane maintained a relatively stable evaporation rate of ∼1.51 kg m^{-1} h^{-1}, with the solar-to-vapor efficiency of around 82% during 10 cycles (Figure S7).

CONCLUSIONS

In summary, we presented a PDA-modified biochar composite membrane for solar steam generation. Due to the advantages of a hierarchically porous structure and large specific surface area, the light absorber can harvest light energy to the maximum

https://dx.doi.org/10.1021/acsomega.9b03718
ACS Omega 2020, 5, 2878−2885

extent (~96%) and convert it into thermal energy. Hydrophilic channels enabled the biochar composite membrane to pump water continuously and generate water vapor more effectively in the process of solar evaporation. The tree-like evaporation configuration with a low-cost advantage realized an evaporation rate of 1.65 kg m^{-2} h^{-1} under 1 sun illumination (1 kW m^{-2}), which allowed the evaporator to achieve a solar-to-vapor conversion efficiency of ~90.5%. In addition, the composite membrane can efficiently remove sodium ions from actual seawater (≥99.9%) and heavy-metal ions from simulated wastewater (≥99.5%). The long-term stable evaporation performance proved its potential in actual solar desalination. More significantly, our work put forward a strategy of recycling and reusing natural biomass waste and broadened their potential application in environmental and energy fields.

EXPERIMENTAL SECTION

Materials. The catkins were collected in May in Heilongjiang University (Harbin, China). Dopamine hydrochloride and tris (hydroxymethyl) aminomethane hydrochlorlde (Tris−HCl) were purchased from Aladdin Chemical Co., Ltd. NaCl, Pb $(NO_3)_2$, $ZnCl_2$, $CuSO_4{\cdot}5H_2O$, $Ni(NO_3)_2{\cdot}6H_2O$, and $Cd(NO_3)_2{\cdot}4H_2O$ were purchased from Sinopharm Chemical Reagent Co., Ltd. Water used in all of the experiments was deionized. The seawater was obtained from the Bohai Sea, China.

Preparation of the Composite Membrane. First, the catkins were washed to remove seeds and dust and then dried at 80 °C for 6 h. A certain mass of white crude catkins was activated by 2 M KOH solution and then dried in 80 °C for 12 h. Subsequently, it was heated to 750 °C at the rate of 5 °C min^{-1} and kept for 1 h under nitrogen atmosphere in a nickel crucible. The resulting solid was repeatedly washed with 1 M HCl and deionized water until the pH value of the filtrate reached about 7. The samples were named as PCPs.

The PCPs were treated using mixed acid (H_2SO_4/HNO_3 = 3:1) for 1 h and then washed by deionized (DI) water until the pH value of the filtrate reached about 7. Subsequently, 15 mg of acidified PCPs were added into dopamine hydrochloride Tris-buffer solution (pH = 8.5, 50 mM) and then stirred for 8 h at 25 °C according to refs 55, 56. The samples were washed by deionized water several times, and they were named as modified PCPs. Finally, the as-prepared product was filtered in a cellulose filter with a thickness of 200 um under a pressure of 0.1 MPa and dried at 60 °C for 4 h.

Characterization. The morphology and structure of the samples were characterized by a scanning electron microscope (S-4800) and a transmission electron microscopy (JEM1005 at 100 kV). The Brunauer−Emmett−Teller (BET) surface area measurement was carried out by nitrogen adsorption−desorption (ASAP 2020). The elements and functional groups of the samples were characterized by X-ray photoelectron spectroscopy (XPS, AXIS Ultra DLD, Kratos) and Fourier transform infrared (FTIR) spectra (ADVANCE III). Contact angle measurement was performed using a contact angle meter (OCA20, Dataphysics) by placing a water droplet (~5 μL) on the surface of the samples. The light source was a 300 W xenon lamp (Micro-solar 300UV, Perfect Light, simulated sunlight source). The light intensity was calibrated by a photo radiometer (PL-MW2000, Perfect Light). Simultaneously, the real-time temperature was monitored by an infrared radiation (IR) camera (FLIR One Pro). The concentrations of ions were measured using an inductively coupled plasma-optical emission spectrometer (Optima 8300, PerkinElmer). The thermal conductivity was evaluated by the Netzsch hyper flash apparatus at room temperature (LFA 467).

Solar Steam Generation Measurement. The composite membrane was cut into a circular shape with a diameter of 20 mm and placed on the polystyrene foam with low thermal conductivity. The above part was fixed on the top of a circular quartz container, which was surrounded by a thermal insulation layer. A rectangle glass filter paper was used as a hydrophilic bridge between the bulk water and the membrane. The whole device was irradiated by a solar simulator under different optical concentrations. The evaporation rates were measured after steadily running for 30 min, and the weight loss was recorded using an electronic mass balance. Temperature changes of the surface of the membrane were monitored using an IR camera. During each test, the ambient temperature was maintained at 24−26 °C, and the ambient humidity was maintained at 45−50%.

ASSOCIATED CONTENT

Supporting Information

The Supporting Information is available free of charge at https://pubs.acs.org/doi/10.1021/acsomega.9b03718.

Atomic contents of C, N, and O elements (atom %); water contact angles of PCPs and modified PCPs; water mass change for the membrane with 15 mg of PCPs and modified PCPs under 1 sun irradiation and with 15 mg of modified PCPs in the dark condition; calculation of the energy conversion efficiency; picture of the solar steam generation in a closed container; mass change of seawater and simulated wastewater versus time under solar illumination of 1 sun; ion rejection of simulated seawater, simulated wastewater and real seawater after solar thermal purification; and cycle performance of the modified-PCPs membrane under 1 sun illumination (PDF)

Web enhanced object (Movie S1) (AVI)

Web enhanced object (Movie S2) (AVI)

AUTHOR INFORMATION

Corresponding Authors

Yanhong Zhang − *School of Chemical Engineering and Materials, Heilongjiang University, Harbin 150080, P. R. China*; Email: zhangyanhong1996@163.com

Liguo Sun − *School of Chemical Engineering and Materials, Heilongjiang University, Harbin 150080, P. R. China*; orcid.org/0000-0002-5584-7204; Email: sunliguo1975@163.com

Authors

Shaochun Zhang − *School of Chemical Engineering and Materials, Heilongjiang University, Harbin 150080, P. R. China*

Linlin Zang − *State Key Laboratory of Urban Water Resource and Environment, School of Environment, Harbin Institute of Technology, Harbin 150090, P. R. China*

Tianwei Dou − *School of Chemical Engineering and Materials, Heilongjiang University, Harbin 150080, P. R. China*

Jinlong Zou − *School of Chemical Engineering and Materials, Heilongjiang University, Harbin 150080, P. R. China*; orcid.org/0000-0003-0651-761X

Complete contact information is available at: https://pubs.acs.org/10.1021/acsomega.9b03718

https://dx.doi.org/10.1021/acsomega.9b03718
ACS Omega 2020, 5, 2878−2885

Author Contributions

All of the authors have given approval to the final version of the paper.

Notes

The authors declare no competing financial interest.

■ ACKNOWLEDGMENTS

The present study was supported by the National Natural Science Foundation of China (51973051 and 51527804) and the Heilongjiang Natural Science Foundation Project (LH2019E077).

■ REFERENCES

(1) Barnaby, W. Do nations go to war over water? *Nature* **2009**, *458*, 282−283.
(2) Elimelech, M.; Phillip, W. A. The Future of Seawater Desalination: Energy, Technology, and the Environment. *Science* **2011**, *333*, 712−717.
(3) Novick, K. A.; Ficklin, D. L.; Stoy, P. C.; Williams, C. A.; Bohrer, G.; Oishi, A. C.; Papuga, S. A.; Blanken, P. D.; Noormets, A.; Sulman, B. N.; Scott, R. L.; Wang, L.; Phillips, R. P. The increasing importance of atmospheric demand for ecosystem water and carbon fluxes. *Nat. Clim. Change* **2016**, *6*, 1023−1027.
(4) Abraham, R.; Mani, A. Heat transfer characteristics in horizontal tube bundles for falling film evaporation in multi-effect desalination system. *Desalination* **2015**, *375*, 129−137.
(5) An, W.; Zhou, X.; Liu, X.; Chai, P. W.; Kuznicki, T.; Kuznicki, S. M. Natural zeolite clinoptilolite-phosphate composite Membranes for water desalination by pervaporation. *J. Membr. Sci.* **2014**, *470*, 431−438.
(6) He, T. X.; Yan, L. J. Application of alternative energy integration technology in seawater desalination. *Desalination* **2009**, *249*, 104−108.
(7) Tao, P.; Ni, G.; Song, C.; Shang, W.; Wu, J.; Zhu, J.; Chen, G.; Deng, T. Solar-driven interfacial evaporation. *Nat. Energy* **2018**, *3*, 1031−1041.
(8) Ghasemi, H.; Ni, G.; Marconnet, A. M.; Loomis, J.; Yerci, S.; Miljkovic, N.; Chen, G. Solar steam generation by heat localization. *Nat. Commun.* **2014**, *5*, No. 4449.
(9) Yang, P.; Liu, K.; Chen, Q.; Li, J.; Duan, J.; Xue, G.; Xu, Z.; Xie, W.; Zhou, J. Solar-driven simultaneous steam production and electricity generation from salinity. *Energy Environ. Sci.* **2017**, *10*, 1923−1927.
(10) Zhao, F.; Zhou, X.; Shi, Y.; Qian, X.; Alexander, M.; Zhao, X.; Mendez, S.; Yang, R.; Qu, L.; Yu, G. Highly efficient solar vapour generation via hierarchically nanostructured gels. *Nat. Nanotechnol.* **2018**, *13*, 489−495.
(11) Zhou, X.; Zhao, F.; Guo, Y.; Zhang, Y.; Yu, G. A hydrogel-based antifouling solar evaporator for highly efficient water desalination. *Energy Environ. Sci.* **2018**, *11*, 1985−1992.
(12) Wang, P. Emerging investigator series: the rise of nano-enabled photothermal materials for water evaporation and clean water production by sunlight. *Environ. Sci.: Nano* **2018**, *5*, 1078−1089.
(13) Dao, V. D.; Choi, H. S. Carbon-Based Sunlight Absorbers in Solar-Driven Steam Generation Devices. *Glob. Challenges* **2018**, *2*, No. 1700094.
(14) Li, Y.; Gao, T.; Yang, Z.; Chen, C.; Luo, W.; Song, J.; Hitz, E.; Jia, C.; Zhou, Y.; Liu, B.; Yang, B.; Hu, L. 3D-Printed, All-in-One Evaporator for High-Efficiency Solar Steam Generation under 1 Sun Illumination. *Adv. Mater.* **2017**, *29*, No. 1700981.
(15) Wang, Y.; Wang, C.; Song, X.; Huang, M.; Megarajan, S. K.; Shaukat, S. F.; Jiang, H. Improved light-harvesting and thermal management for efficient solar-driven water evaporation using 3D photothermal cones. *J. Mater. Chem. A* **2018**, *6*, 9874−9881.
(16) Zhang, L.; Xing, J.; Wen, X.; Chai, J.; Wang, S.; Xiong, Q. Plasmonic heating from indium nanoparticles on a floating microporous membrane for enhanced solar seawater desalination. *Nanoscale* **2017**, *9*, 12843−12849.
(17) Chen, M.; Wu, Y.; Song, W.; Mo, Y.; Lin, X.; He, Q.; Guo, B. Plasmonic nanoparticle-embedded poly(p-phenylene benzobisoxazole) nanofibrous composite films for solar steam generation. *Nanoscale* **2018**, *10*, 6186−6193.
(18) Wang, G.; Fu, Y.; Ma, X.; Pi, W.; Liu, D.; Wang, X. Reusable reduced graphene oxide based double-layer system modified by polyethylenimine for solar steam generation. *Carbon* **2017**, *114*, 117−124.
(19) Wang, G.; Fu, Y.; Guo, A.; Mei, T.; Wang, J.; Li, J.; Wang, X. Reduced Graphene Oxide−Polyurethane Nanocomposite Foam as a Reusable Photoreceiver for Efficient Solar Steam Generation. *Chem. Mater.* **2017**, *29*, 5629−5635.
(20) Wang, Y.; Zhang, L.; Wang, P. Self-Floating Carbon Nanotube Membrane on Macroporous Silica Substrate for Highly Efficient Solar-Driven Interfacial Water Evaporation. *ACS Sustainable Chem. Eng.* **2016**, *4*, 1223−1230.
(21) Yin, Z.; Wang, H.; Jian, M.; Li, Y.; Xia, K.; Zhang, M.; Wang, C.; Wang, Q.; Ma, M.; Zheng, Q. S.; Zhang, Y. Extremely Black Vertically Aligned Carbon Nanotube Arrays for Solar Steam Generation. *ACS Appl. Mater. Interfaces* **2017**, *9*, 28596−28603.
(22) Lin, X.; Chen, J.; Yuan, Z.; Yang, M.; Chen, G.; Yu, D.; Zhang, M.; Hong, W.; Chen, X. Integrative solar absorbers for highly efficient solar steam generation. *J. Mater. Chem. A* **2018**, *6*, 4642−4648.
(23) Shi, L.; Shi, Y.; Li, R.; Chang, J.; Zaouri, N.; Ahmed, E.; Jin, Y.; Zhang, C.; Zhuo, S.; Wang, P. SiC−C Composite as a Highly Stable and Easily Regenerable Photothermal Material for Practical Water Evaporation. *ACS Sustainable Chem. Eng.* **2018**, *6*, 8192−8200.
(24) Xu, Y.; Ma, J.; Han, Y.; Zhang, J.; Cui, F.; Zhao, Y.; Li, X.; Wang, W. Multifunctional CuO Nanowire Mesh for Highly Efficient Solar Evaporation and Water Purification. *ACS Sustainable Chem. Eng.* **2019**, *7*, 5476−5485.
(25) Singh, S.; Shauloff, N.; Jelinek, R. Solar-Enabled Water Remediation via Recyclable Carbon Dot/Hydrogel Composites. *ACS Sustainable Chem. Eng.* **2019**, *7*, 13186−13194.
(26) Dong, T.; Xu, G.; Wang, F. Adsorption and adhesiveness of kapok fiber to different oils. *J. Hazard. Mater.* **2015**, *296*, 101−111.
(27) Deng, J.; Yang, B.; Chen, C.; Liang, J. Renewable Eugenol-Based Polymeric Oil-Absorbent Microspheres: Preparation and Oil Absorption Ability. *ACS Sustainable Chem. Eng.* **2015**, *3*, 599−605.
(28) Yang, S.; Chen, L.; Mu, L.; Hao, B.; Ma, P. C. Low cost carbon fiber aerogel derived from bamboo for the adsorption of oils and organic solvents with excellent performances. *RSC Adv.* **2015**, *5*, 38470−38478.
(29) Li, Y. Q.; Samad, Y. A.; Polychronopoulou, K.; Alhassan, S. M.; Liao, K. Carbon Aerogel from Winter Melon for Highly Efficient and Recyclable Oils and Organic Solvents Absorption. *ACS Sustainable Chem. Eng.* **2014**, *2*, 1492−1497.
(30) Yahya, M. A.; Al-Qodah, Z.; Ngah, C. W. Z. Agricultural bio-waste materials as potential sustainable precursors used for activated carbon production: A review. *Renewable Sustainable Energy Rev.* **2015**, *46*, 218−235.
(31) Zhu, M.; Yu, J.; Ma, C.; Zhang, C.; Wu, D.; Zhu, H. Carbonized daikon for high efficient solar steam generation. *Sol. Energy Mater. Sol. Cells* **2019**, *191*, 83−90.
(32) Xue, G.; Liu, K.; Chen, Q.; Yang, P.; Li, J.; Ding, T.; Duan, J.; Qi, B.; Zhou, J. Robust and Low-Cost Flame-Treated Wood for High-Performance Solar Steam Generation. *ACS Appl. Mater. Interfaces* **2017**, *9*, 15052−15057.
(33) Li, T.; Liu, H.; Zhao, X.; Chen, G.; Dai, J.; Pastel, G.; Jia, C.; Chen, C.; Hitz, E.; Siddhartha, D.; Yang, R.; Hu, L. Scalable and Highly Efficient Mesoporous Wood-Based Solar Steam Generation Device: Localized Heat, Rapid Water Transport. *Adv. Funct. Mater.* **2018**, *28*, No. 1707134.
(34) Xu, N.; Hu, X.; Xu, W.; Li, X.; Zhou, L.; Zhu, S.; Zhu, J. Mushrooms as Efficient Solar Steam-Generation Devices. *Adv. Mater.* **2017**, *29*, No. 1606762.
(35) Liu, H.; Chen, C.; Chen, G.; Kuang, Y.; Zhao, X.; Song, J.; Jia, C.; Xu, X.; Hitz, E.; Xie, H.; Wang, S.; Jiang, F.; Li, T.; Li, Y.; Gong, A.; Yang, R.; Das, S.; Hu, L. High-Performance Solar Steam Device with

https://dx.doi.org/10.1021/acsomega.9b03718
ACS Omega 2020, 5, 2878−2885

Layered Channels: Artificial Tree with a Reversed Design. *Adv. Energy Mater.* **2018**, *8*, No. 1701616.
(36) Luo, X.; Huang, C.; Liu, S.; Zhong, J. High performance of carbon-particle/bulk-wood bi-layer system for solar steam generation. *Int. J. Energy Res.* **2018**, *42*, 4830−4839.
(37) Zhu, M.; Li, Y.; Chen, F.; Zhu, X.; Dai, J.; Li, Y.; Yang, Z.; Yan, X.; Song, J.; Wang, Y.; Hitz, E.; Luo, W.; Lu, M.; Yang, B.; Hu, L. Plasmonic Wood for High-Efficiency Solar Steam Generation. *Adv. Energy Mater.* **2018**, *8*, No. 1701028.
(38) Chen, C.; Li, Y.; Song, J.; Yang, Z.; Kuang, Y.; Hitz, E.; Jia, C.; Gong, A.; Jiang, F.; Zhu, J. Y.; Yang, B.; Xie, J.; Hu, L. Highly Flexible and Efficient Solar Steam Generation Device. *Adv. Mater.* **2017**, *29*, No. 1701756.
(39) Wang, Y.; Liu, H.; Chen, C.; Kuang, Y.; Song, J.; Xie, H.; Jia, C.; Kronthal, S.; Xu, X.; He, S.; Hu, L. All Natural, High Efficient Groundwater Extraction via Solar Steam/Vapor Generation. *Adv. Sustainable Syst.* **2018**, *3*, No. 1800055.
(40) Liu, K. K.; Jiang, Q.; Tadepalli, S.; Raliya, R.; Biswas, P.; Naik, R. R.; Singamaneni, S. Wood-Graphene Oxide Composite for Highly Efficient Solar Steam Generation and Desalination. *ACS Appl. Mater. Interfaces* **2017**, *9*, 7675−7681.
(41) Chen, B.; Ma, Q.; Tan, C.; Lim, T. T.; Huang, L.; Zhang, H. Carbon-Based Sorbents with Three-Dimensional Architectures for Water Remediation. *Small* **2015**, *11*, 3319−3336.
(42) Fang, J.; Liu, J.; Gu, J.; Liu, Q.; Zhang, W.; Su, H.; Zhang, D. Hierarchical Porous Carbonized Lotus Seedpods for Highly Efficient Solar Steam Generation. *Chem. Mater.* **2018**, *30*, 6217−6221.
(43) Kuang, Y.; Chen, C.; He, S.; Hitz, E. M.; Wang, Y.; Gan, W.; Mi, R.; Hu, L. A High-Performance Self-Regenerating Solar Evaporator for Continuous Water Desalination. *Adv. Mater.* **2019**, *31*, No. 1900498.
(44) Liu, F.; Zhao, B.; Wu, W.; Yang, H.; Ning, Y.; Lai, Y.; Bradley, R. Low Cost, Robust, Environmentally Friendly Geopolymer-Mesoporous Carbon Composites for Efficient Solar Powered Steam Generation. *Adv. Funct. Mater.* **2018**, *28*, No. 1803266.
(45) Bai, X.; Li, Y.; Zhang, F.; Xu, Y.; Wang, S.; Fu, G. Mass production of superhydrophilic sponges for efficient and stable solar-driven highly corrosive water evaporation. *Environ. Sci.: Water Res. Technol.* **2019**, *5*, 2041−2047.
(46) Liang, H.; Liao, Q.; Chen, N.; Liang, Y.; Lv, G.; Zhang, P.; Lu, B.; Qu, L. Thermal efficiency of solar steam generation approaching 100% through capillary water transport. *Angew. Chem.* **2019**, *131*, 19217−19222.
(47) Zhou, X.; Zhao, F.; Guo, Y.; Zhang, Y.; Yu, G. A hydrogel-based antifouling solar evaporator for highly efficient water desalination. *Energy Environ. Sci.* **2018**, *11*, 1985−1992.
(48) Wu, X.; Chen, G. Y.; Zhang, W.; Liu, X.; Xu, H. A Plant-Transpiration-Process-Inspired Strategy for Highly Efficient Solar Evaporation. *Adv. Sustainable Syst.* **2017**, *1*, No. 1700046.
(49) Zang, L.; Bu, Z.; Sun, L.; Zhang, Y. Hollow carbon fiber sponges from crude catkins: an ultralow cost absorbent for oils and organic solvents. *RSC Adv.* **2016**, *6*, 48715−48719.
(50) Wang, K.; Zhao, N.; Lei, S.; Yan, R.; Tian, X.; Wang, J.; Song, Y.; Xu, D.; Guo, Q.; Liu, L. Promising biomass-based activated carbons derived from willow catkins for high performance supercapacitors. *Electrochim. Acta* **2015**, *166*, 1−11.
(51) Zhang, Y.; Zhao, Y.; Konarov, A.; Li, Z.; Chen, P. Effect of mesoporous carbon microtube prepared by carbonizing the poplar catkin on sulfur cathode performance in Li/S batteries. *J. Alloys Compd.* **2015**, *619*, 298−302.
(52) Xie, L.; Sun, G.; Su, F.; Guo, X.; Kong, Q.; Li, X.; Huang, X.; Wan, L.; song, W.; Li, K.; Lv, C.; Chen, C.-M. Hierarchical porous carbon microtubes derived from willow catkins for supercapacitor applications. *J. Mater. Chem. A* **2016**, *4*, 1637−1646.
(53) Finnerty, C.; Zhang, L.; Sedlak, D. L.; Nelson, K. L.; Mi, B. Synthetic Graphene Oxide Leaf for Solar Desalination with Zero Liquid Discharge. *Environ. Sci. Technol.* **2017**, *51*, 11701−11709.
(54) Mi, B.; Finnerty, C.; Conway, K. Prospects of artificial tree for solar desalination. *Curr. Opin. Chem. Eng.* **2019**, *25*, 18−25.
(55) Zhang, C.; Ma, M. Q.; Chen, T. T.; Zhang, H.; Hu, D. F.; Wu, B. H.; Ji, J.; Xu, Z. K. Dopamine-Triggered One-Step Polymerization and Codeposition of Acrylate Monomers for Functional Coatings. *ACS Appl. Mater. Interfaces* **2017**, *9*, 34356−34366.
(56) Xing, R.; Wang, W.; Jiao, T.; Ma, K.; Zhang, Q.; Hong, W.; Qiu, H.; Zhou, J.; Zhang, L.; Peng, Q. Bioinspired Polydopamine Sheathed Nanofibers Containing Carboxylate Graphene Oxide Nanosheet for High-Efficient Dyes Scavenger. *ACS Sustainable Chem. Eng.* **2017**, *5*, 4948−4956.
(57) Zang, L.; Cao, X.; Zhang, Y.; Sun, L.; Qin, C.; Wang, C. Microfluidic generation of graphene beads for supercapacitor electrode materials. *J. Mater. Chem. A* **2015**, *3*, 22088−22093.
(58) Abioye, A. M.; Ani, F. N. Recent development in the production of activated carbon electrodes from agricultural waste biomass for supercapacitors: A review. *Renewable Sustainable Energy Rev.* **2015**, *52*, 1282−1293.
(59) Deng, H.; Li, G.; Yang, H.; Tang, J.; Tang, J. Preparation of activated carbons from cotton stalk by microwave assisted KOH and K_2CO_3 activation. *Chem. Eng. J.* **2010**, *163*, 373−381.
(60) Sevilla, M.; Fuertes, A. B. Sustainable porous carbons with a superior performance for CO_2 capture. *Energy Environ. Sci.* **2011**, *4*, 1765−1771.
(61) Ito, Y.; Tanabe, Y.; Han, J.; Fujita, T.; Tanigaki, K.; Chen, M. Multifunctional Porous Graphene for High-Efficiency Steam Generation by Heat Localization. *Adv. Mater.* **2015**, *27*, 4302−4307.
(62) Ge, H.; Wang, J. Ear-like poly (acrylic acid)-activated carbon nanocomposite: A highly efficient adsorbent for removal of Cd(II) from aqueous solutions. *Chemosphere* **2017**, *169*, 443−449.
(63) Wu, X.; Wu, L.; Tan, J.; Chen, G. Y.; Owens, G.; Xu, H. Evaporation above a bulk water surface using an oil lamp inspired highly efficient solar-steam generation strategy. *J. Mater. Chem. A* **2018**, *6*, 12267−12274.
(64) Jiang, Q.; Derami, H. G.; Ghim, D.; Cao, S.; Jun, Y. S.; Singamaneni, S. Polydopamine-filled bacterial nanocellulose as a biodegradable interfacial photothermal evaporator for highly efficient solar steam generation. *J. Mater. Chem. A* **2017**, *5*, 18397−18402.
(65) Liu, G.; Xu, J.; Wang, K. Solar water evaporation by black photothermal sheets. *Nano Energy* **2017**, *41*, 269−284.
(66) He, J.; Zhao, G.; Mu, P.; Wei, H.; Su, Y.; Sun, H.; Zhu, Z.; Liang, W.; Li, A. Scalable fabrication of monolithic porous foam based on cross-linked aromatic polymers for efficient solar steam generation. *Sol. Energy Mater. Sol. Cells* **2019**, *201*, No. 110111.
(67) Fan, Y.; Bai, W.; Mu, P.; Su, Y.; Zhu, Z.; Sun, H.; Liang, W.; Li, A. Conductively monolithic polypyrrole 3-D porous architecture with micron-sized channels as superior salt-resistant solar steam generators. *Sol. Energy Mater. Sol. Cells* **2020**, *206*, No. 110347.
(68) Mu, P.; Bai, W.; Fan, Y.; Zhang, Z.; Sun, H.; Zhu, Z.; Liang, W.; Li, A. Conductive hollow kapok fiber-PPy monolithic aerogels with excellent mechanical robustness for efficient solar steam generation. *J. Mater. Chem. A* **2019**, *7*, 9673−9679.

https://dx.doi.org/10.1021/acsomega.9b03718
ACS Omega 2020, 5, 2878−2885